Pure Appl. Chem., Vol. 81, No. 12, pp. 2253–2263, 2009.
doi:10.1351/PAC-CON-09-01-13

Formation of ($FeCl_3$)@phenylazomethine dendrimer (DPA): Fine control of the release and encapsulation of Fe ions in dendrimers*

Kimihisa Yamamoto[1,‡], Reina Nakajima[1], Yousuke Ochi[1], Masanori Tsuruta[1], Masayoshi Higuchi[1], Akira Hida[2], and Jun Onoe[2]

[1]Department of Chemistry, Faculty of Science and Technology, Keio University, Yokohama 223-8522, Japan; [2]Research Laboratory for Nuclear Reactors, Tokyo Institute of Technology, 2-12-1 Ookayama, Meguro, Tokyo 152-8550, Japan

Abstract: Phenylazomethine dendrimers (DPAs) act as a strong coordination site for metal ion assembly. DPA G4 is regarded as a molecular capsule having 30 metal-assembling sites with a 2.7 nm diameter. We have reported the radial stepwise complexation with Sn^{2+} ions in the dendrimers, which means the location and number of metal ions can be controlled. Therefore, DPA G4 should realize a ferritin-like redox nanocapsule with precise control of the number of Fe ions. On the other hand, the Fe ion is a typical paramagnetic molecule. For creating an advanced memory with a high density, ferritin is one of the candidates for use as a magnetic quantum dot. Many attempts to use biomaterials, for example, ferritins and chaperonins, as metal storage capsules have been demonstrated. Some research groups fabricate a device by assembling ferritins on a plate using their rigid and uniform structure. The attempts to use dendrimers have also been demonstrated. We now describe the successful attempt to control the "encapsulation and release" of iron ions in a dendrimer in order to mimic a ferritin through the redox reaction. Furthermore, the assembling structures of $(FeCl_3)_n$@DPA on a plate were first observed by scanning tunneling microscopy (STM) as a dendrimer complex, which shows that a highly oriented film is formed on a plate only by solvent casting.

Keywords: assembling structure; encapsulation and release; iron; phenylazomethine dendrimer; precise metal assembly.

INTRODUCTION

Dendrimers have a regular branching structure from the core to the periphery, in which the number of branches sequentially increases as the generation of the dendrimers increases (Fig. 1) [1–5]. Therefore, the shape is close to spherical in the higher-generation dendrimers with a nanospace in the interior of the molecule. We can use the nanocapsules, whose periphery is densely packed, while the core is less crowded. Many investigations are now underway to investigate the selective chemical reactions and drug delivery capsules using a nanospace in a dendrimer [6–9]. To develop an advanced drug delivery system, a controllable response is strongly desired, which makes it possible to precisely control the release and encapsulation of drugs.

*Paper based on a presentation at the International Symposium on Novel Materials and their Synthesis (NMS-IV) and the 18th International Symposium on Fine Chemistry and Functional Polymers (FCFP-XVIII), 15–18 October 2008, Zhenjiang, China. Other presentations are published in this issue, pp. 2253–2424.

‡Corresponding author

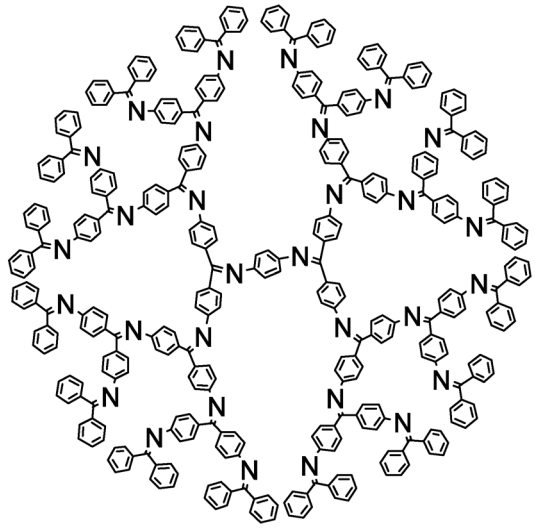

Fig. 1 DPA G4 (dendritic polyphenylazomethine, phenylazomethine dendrimer).

Iron is one of the body's essential elements. Hemoglobin uses Fe ions to bind oxygen molecules. In the body, there is an Fe storage protein called ferritin that contains irons in a nanospace surrounded by protein [10,11]. When Fe is excessive, it is encapsulated into the ferritin. When it is scarce, it is released from the ferritin. These encapsulations and the releases of Fe are controlled by the redox couple Fe^{2+}/Fe^{3+}. Fe^{2+} is oxidized to Fe^{3+} through the protein shell and encapsulated into the ferritin. Fe^{3+} is released after its reduction by an enzyme. This redox switching of the encapsulation and the release has already been reported in a small molecular system. However, it is quite difficult to precisely control it in a macromolecular system like polymers and proteins. The compulsory release and encapsulation of irons from natural ferritins using an electrode has been studied, but it has been difficult to detect the exact phenomenon. Rao et al. have reported the ferritin core analogs in sol-gel system, however, its size was not precisely uniformed [12]. The nanoparticles consist of 700–4000 Fe atoms with 4–7 nm diameters.

COMPLEXATION BEHAVIOR BETWEEN DPA AND Fe IONS

Imine groups have C=N double bonds that can form a complex with various metals. In this article, the complexation behaviors of Fe ions, especially Fe^{2+} and Fe^{3+}, will be described. Phenylazomethine dendrimer (DPA) G0 that has one imine group was synthesized as a model compound.

The complexation of DPA G0 and $FeCl_3$ in a chloroform/acetonitrile mixed solvent (v/v 1:1) was observed by UV–vis spectroscopy. A Job plot shows a maximum at a 0.5 mol fraction of DPA G0, i.e., the imine forms a 1:1 imine/$FeCl_3$ complex (Fig. 2) [13]. The association constant, $K_{Fe^{3+}}$, was determined to be more than 108 [M^{-1}], which is 100 times greater than that of $SnCl_2$ (cf. 9.6×10^5 M^{-1}), by curve-fitting a theoretical simulation to the experimental data. This indicates that a quantitative complexation between the imine group and $FeCl_3$ is obtained below the concentration of 10^{-6} M for UV–vis spectroscopy.

When $FeCl_2$ was added to the DPA G0 solution, the spectra did not change under the UV–vis spectroscopic conditions. The equilibrium constant, $K_{Fe^{2+}}$, was determined by a chemical shift in the ^1H NMR. In $CDCl_3/CD_3CN$ mixed solvent, the $FeCl_2$-DPA G0 mixtures in various proportions were prepared. When the [Fe]/[G0] increased, a downfield shift was observed. The chemical shifts of DPA G0 are the weighted average of the chemical shift of the free DPA G0 and the complex under the con-

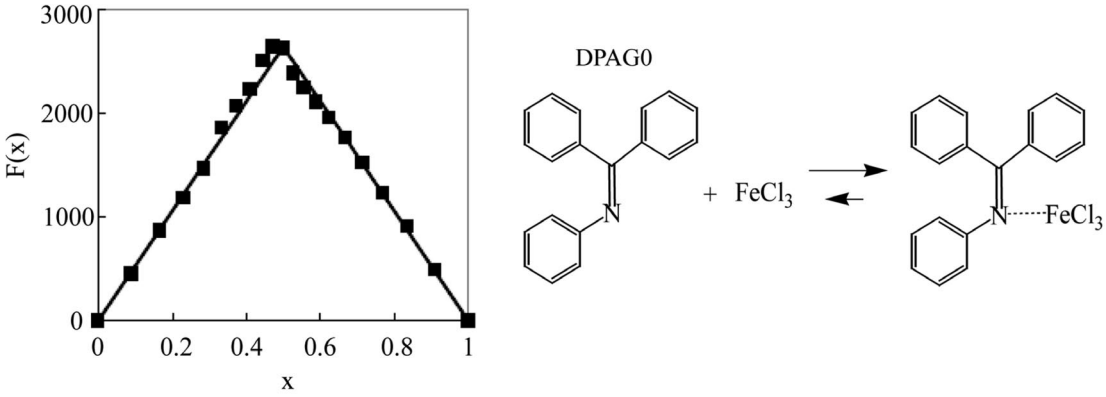

Fig. 2 A Job plot of $FeCl_3$ and DPA G0. $F(x) = Abs/(C_{G0} + C_{FeCl_3}) - (\varepsilon_{G0}\ \varepsilon_{FeCl_3})x - \varepsilon_{FeCl_3}$, $x = C_{G0}/(C_{G0} + C_{FeCl_3})$ molar fraction of DPA G0. The solution of DPA G0 and $FeCl_3$ (with same concentration, 3.45×10^{-4} M) in chloroform/acetonitrile (1/1) were mixed in various proportions. The plot shows a maximum at a 0.5 mole fraction of DPA G0. This means that the imine forms a 1:1 complex with $FeCl_3$. The equilibrium constant of complexation, K, was determined to be more than 10^8 [M^{-1}] by curve-fitting a theoretical simulation to the experimental data.

ditions that the exchange is fast enough on the NMR time scale. The association constant, $K_{Fe^{2+}}$, was calculated ($K_{Fe^{2+}}$ = ca. 0.8 M^{-1}, δc = ca. 2750 Hz). $K_{Fe^{2+}}$ is 108 times smaller than $K_{Fe^{3+}}$. $FeCl_2$ is not coordinated to DPA G0 under the UV–vis spectroscopic conditions.

RADICAL STEPWISE COMPLEXATION OF DPA AND Fe IONS

We previously succeeded in establishing the precise assembly of metal ions on DPAs [14,15]. DPAs G0–G4 were synthesized using the convergent method through the dehydration of aromatic ketones with aromatic amines in the presence of titanium(IV) tetrachloride [15]. Thirty $FeCl_3$ molecules should be assembled on 30 imine groups in the fourth generation of dendritic polyphenylazomethine (DPA G4), because $FeCl_3$ is quantitatively coordinated on the imine group [16]. The complexation behaviors between DPAs G0–G4 and $FeCl_3$ were observed by UV–vis spectroscopy. During the addition of $FeCl_3$, the color of the DPA G2 solution changed from yellow to orange due to the complexation. However, no isosbestic point was observed (Fig. 3a).

$FeCl_3$ has an absorbance at λ_{max} = 310 and 360 nm (i.e., $\varepsilon_M \neq 0$). When subtracting the absorbance of the metal ($\varepsilon_M[M]_t$) from each spectra (Fig. 3b), an isosbestic point is observed. A decrease in the π–π* absorption of the imine bonds at 285 nm and an increase in the absorption of a complex at 410 nm are observed. During the addition of 2 equiv of $FeCl_3$, the isosbestic point is observed at 348 nm. Upon the addition between 3–6 equiv of $FeCl_3$, the isosbestic point shifted to 357 nm. This indicates that there are imine sites with two different chemical environments in the system. The number of added equivalents of $FeCl_3$ to induce the shifts in the isosbestic points is in good agreement with the number of imine sites for each generation of DPA G2.

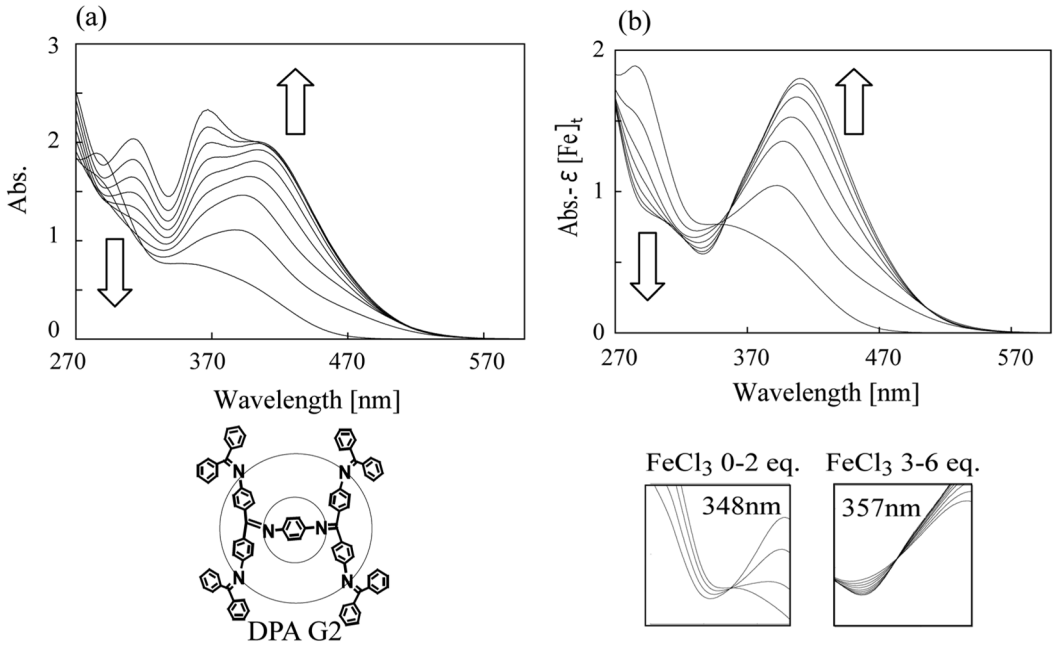

Fig. 3 (a) UV–vis spectra changes of DPA G2 (2.72×10^{-5} M) complexed with 0–6 equiv of $FeCl_3$ in acetonitrile:chloroform = 1:1. (b) Spectra after subtracting the absorption of Fe^{3+} from (a). (Under) Enlargements focusing on the isosbestic points.

$FeCl_3$ was also added to DPA G4 (Fig. 4). After subtraction of the absorption of $FeCl_3$, the absorbance around 335 nm attributed to the imine groups decreased and the absorbance around 410 nm attributed to the complex increased. The isosbestic point shifted in four steps during the addition of 30 equiv of $FeCl_3$ (0–2 equiv; 374 nm, 3–6 equiv; 367 nm, 7–14 equiv; 365 nm, 15–30 equiv; 364 nm). The number of added equivalents of $FeCl_3$ for inducing the shifts is in good agreement with the number of imine sites for each generation of DPA G4. These results indicate that the complexation proceeds from the core imines to the periphery of DPA G4. A similar stepwise radial complexation was also observed in DPAs G1 and G3. The Fe^{3+} ions are incorporated into the DPAs in a radial stepwise fashion.

Characterization of the $FeCl_3$@DPA complex was carried out by matrix-assisted laser desorption/ionization with time-of-flight mass spectroscopy (MALDI-TOF-MS). The molecular fragments of $(FeCl_3)_{30}$@DPA G4 were not detected because of the low ionization activity of the complex. The molecular fragments of $(FeCl_3)_6$@DPA G2 (calcd; $1153.49 + 6 \times 162.21$) were observed at 1153.8, 1317.5, 1481.6, 1645.3, 1807.8, and 1974.6. This result indicates that $3Cl^-$ and one imine of DPA are coordinated to Fe^{3+}. Furthermore, the exact masses of $(FeCl_3)_2$@DPA G2 and $(FeCl_3)_2$@DPA G3 were also determined by MALDI-TOF-MS.

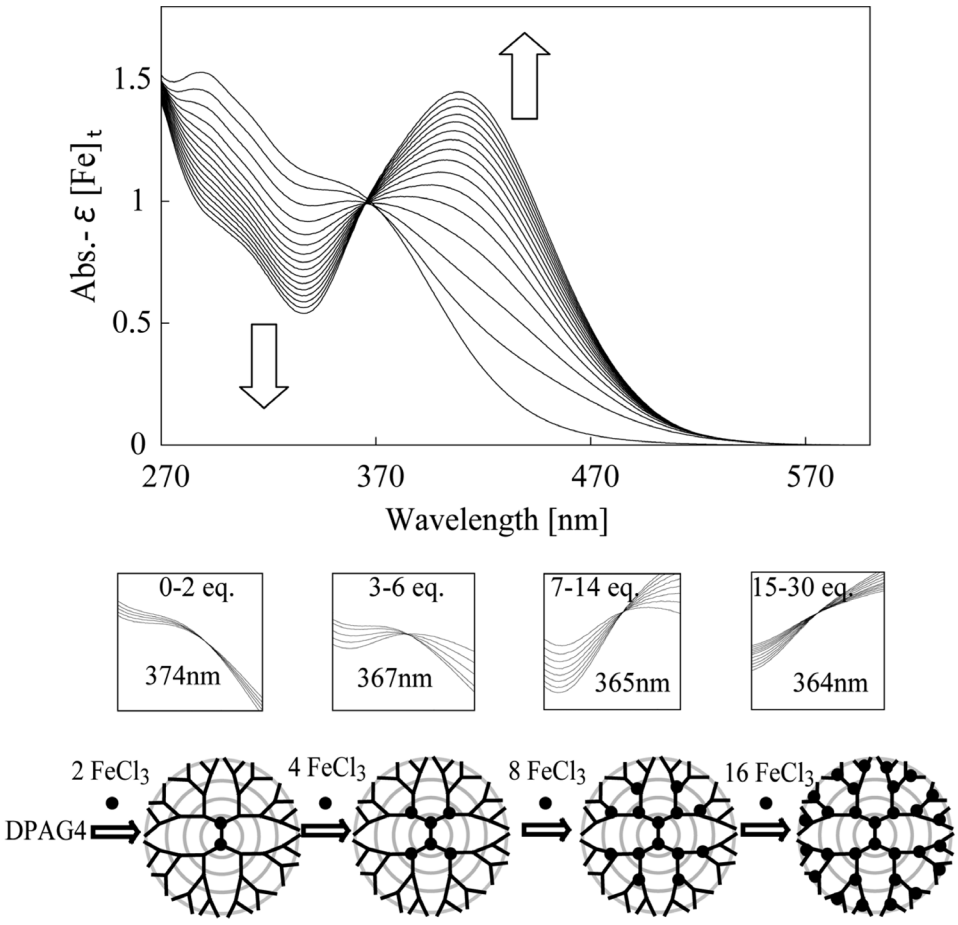

Fig. 4 UV–vis spectra changes of DPA G4 (5.62×10^{-6} M) complexed with 0–30 equiv of $FeCl_3$. (Under) Enlargements focusing on the isosbestic points and scheme of radial complexation fashion.

Furthermore, the electrochemical analysis of the Fe ions in DPA also indicates the precise assembly of the Fe ions in DPA G4 by cyclic voltammetry. The reversible redox wave of the Fe^{2+}/Fe^{3+} couple in $(FeCl_3)_2$@DPA G1 was observed at –0.28 V vs. Fc/Fc^+ in a chloroform/acetonitrile (v/v 1/1) mixed solvent under an argon atmosphere. However, for $(FeCl_3)_2$@DPA G4, a redox wave became irreversible, which has a large peak potential separation (Fig. 5a, ΔE_p = 160 mV, scan rate 0.1 V/s). The peak potentials upon changing the scan rates were fitted to the simulation data from Digisim to determine the electron-transfer rates, k_s [17]. The electron-transfer rate of $(FeCl_3)_2$@DPA G4 and $(FeCl_3)_{30}$@DPA G4 were determined to be 0.0015 cm s^{-1} and 0.015 cm s^{-1}, respectively. Since the deformation of the DPA G4 molecules is small due to their rigid structure, the distance between the Fe in the dendrimer and the electrode is regarded as constant during the redox reaction (Fig. 5c). The results mean that for $(FeCl_3)_2$@DPA G4, 2 Fe ions are coordinated to the imine groups near the core. In the $(FeCl_3)_2$@DPA G4, the electron transfer is drastically suppressed due to the shell effect because 2 iron ions complexed with the imine sites at the first layer are separated from the electrode by more than 1 nm (Fig. 5c). The k_s values of $(FeCl_3)_6$@DPA G4 and $(FeCl_3)_{14}$@DPA G4 were determined to be 0.006 and 0.010 cm s^{-1}, respectively. The distance between the electrode and Fe ions was estimated by the molecular modeling. A plot of the electron-transfer rates vs. the distance between the electrode and each generation layer in DPA G4 gives a straight line (Fig. 5b). The electron-transfer process in

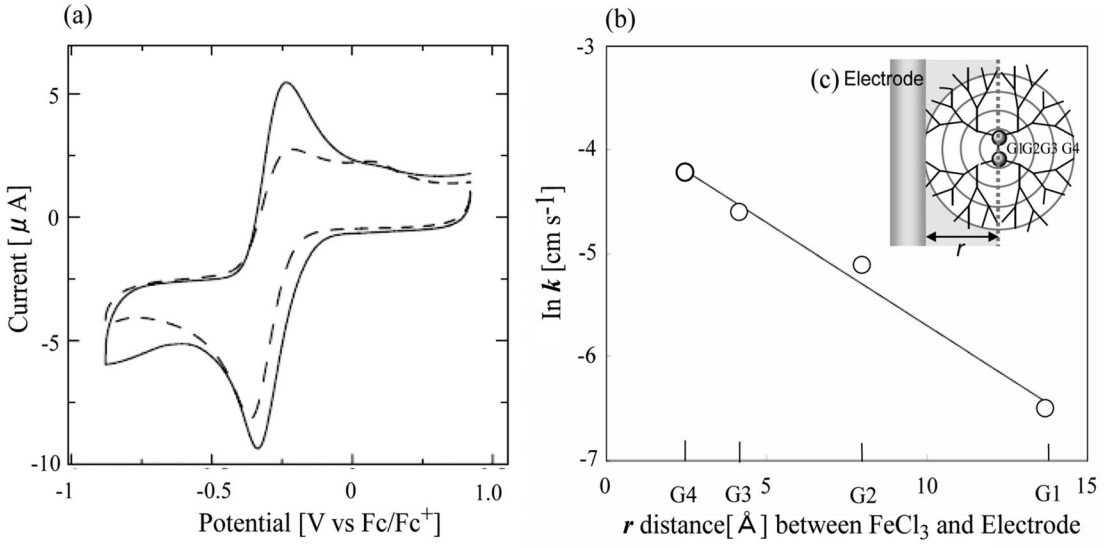

Fig. 5 (a) Cyclic voltammograms of $(FeCl_3)$n@DPA G4. The concentration of $FeCl_3$ in each solution is 0.5 mM. Solid line: $(FeCl_3)_{30}$@DPA G4, dashed line: $(FeCl_3)_{30}$@DPA G4. Scan rate: 0.1 V/s. (b) Plot of ln (k_s [cm s^{-1}]; electron-transfer rate constants of $(FeCl_3)_n$@DPA G4 [n = 2, 6, 14, 30]) vs. distance [Å] from outer shell to the imine site that complexes with $FeCl_3$. The slope is –0.20 $Å^{-1}$. (c) An image of the electron transfer through the shell of $(FeCl_3)_2$@DPA G4.

$(FeCl_3)_n$@DPA G4 obeys the through tunneling theory [18] (ln$k = \beta$d, β; attenuation factor). Chasse et al. had also reported the relationship between the dendrimer's generation and the electron-transfer rates [19]. These results also support the idea that the Fe ion is precisely assembled in the dendrimer from the core to the periphery.

ELIMINATION OF Fe IONS FROM DPA COMPLEXES

The release of $FeCl_3$ is also expected to occur in a stepwise fashion due to the gradient of the imine groups' electron density. Stronger ligands (or stronger Lewis bases) than the imine sites were used for the elimination of $FeCl_3$ from Fe@DPA. Tetrabutylammonium chloride (TBACl) efficiently forms the complex $FeCl_4^-$ and Cl^- bears no large steric hinderance. During the addition of Cl^- to the $(FeCl_3)_2$@DPA G1 solution, the absorption of the complex decreased, which means that a reverse spectra change was observed (Fig. 6a). This behavior consists of two equilibriums as follows:

$$FeCl_3 + \text{imine} = FeCl_3@\text{imine} \qquad K_{\text{imine}}$$

$$FeCl_3 + Cl^- = FeCl_4^- \qquad K_{Cl}$$

The isosbestic points are observed at 338 and 380 nm during the titration of TBACl. The association constant between $FeCl_3$ and Cl^- was determined by curve-fitting with the absorption changes during the titration (Fig. 6b, when K_{imine} is 10^8 M^{-1}, K_{Cl} is 10^9 M^{-1}). This bacisity of Cl^- is strong enough to quantitatively dissociate the Fe ions at the periphery of DPA G4. However, the dissociation of Fe ions from the first layer is difficult due to the strong Lewis basicity of the imine sites.

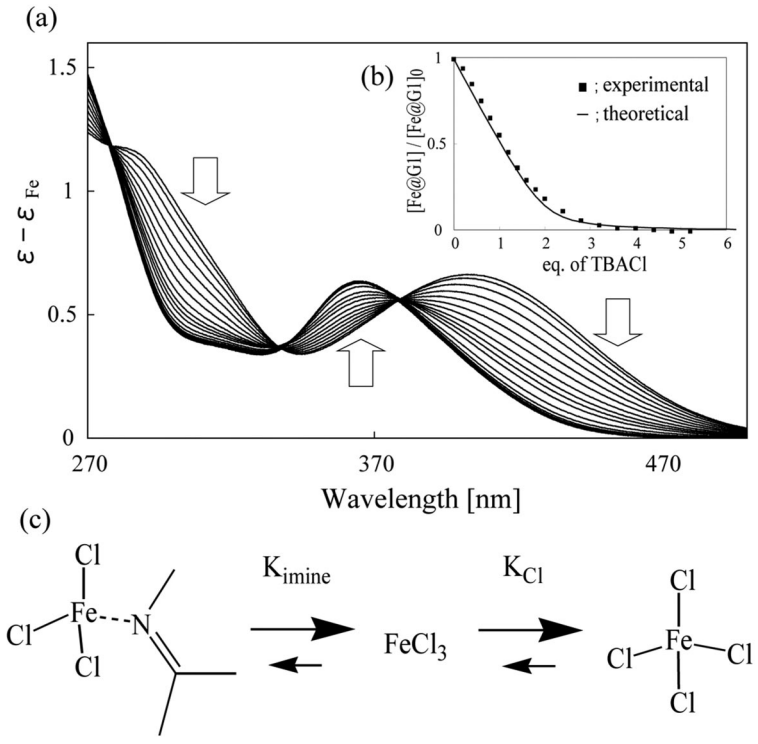

Fig. 6 (a) UV–vis spectra changes of $(FeCl_3)_2$@DPA G1 (5.6×10^{-5} M) + TBACl. (b) Absorption changes at 480 nm. By curve-fitting theoretical simulation, K_{Cl^-} is determined to be 10^9 M^{-1} when K_{imine} is 10^8 M^{-1}. (c) Scheme of dissociation of Fe@imine complex.

After the addition of TBACl to the solution of $(FeCl_3)_{30}$@DPA G4, the absorption of the complex around 410 nm decreased (Fig. 7a), which is similar to that of $(FeCl_3)_2$@DPA G1. An isosbestic point is observed at 365 nm during the addition of 16 equiv of Cl^- and then shifted to 366 nm for the next 8 equiv (Fig. 7b). These equivalents of Cl^- agree with the equivalents of the Fe ions coordinated to the imines in the fourth and third layers. During the following addition, the absorption of the complex decreased. However, quantitative elimination of the Fe ions from the imine sites in the second and first layers was unsuccessful due to the strong basicity of the inner imines when TBACl was used as a base.

Similarly, during the addition of TBACl to the solution of $(FeCl_3)_{14}$@DPA G3, the quantitative elimination of the Fe ions from the third layer was observed, which is confirmed by the observation of an isosbestic point. However, it was also hard to remove the Fe ions from the second and first layers. These results indicated that the release of the Fe^{3+} ions stepwise occurs from the peripheral imines to the core imines.

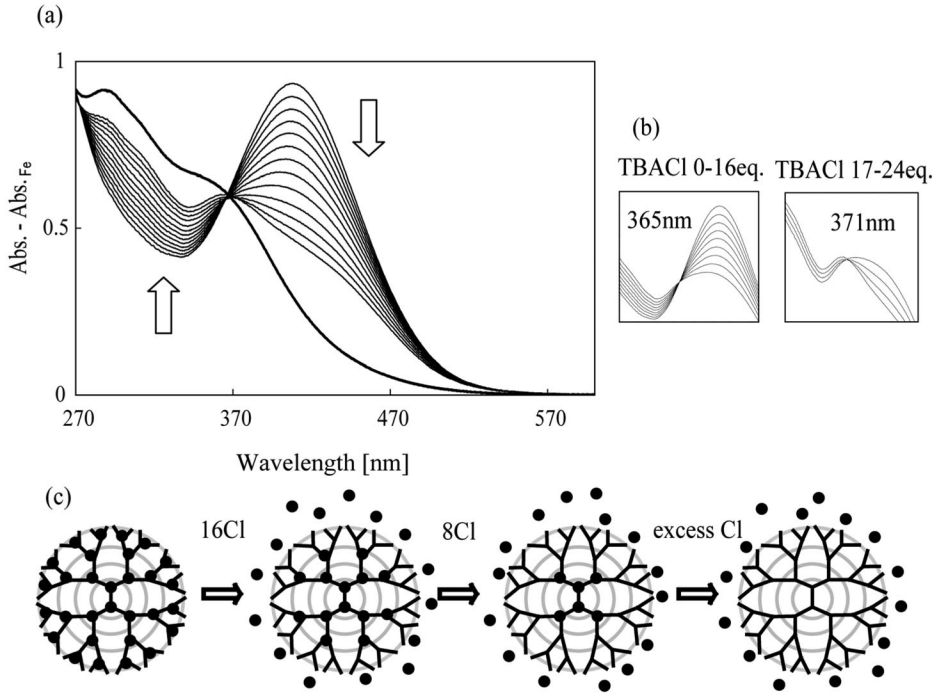

Fig. 7 (a) UV–vis spectra changes of $(FeCl_3)_{30}$@DPA G4 (3.38×10^{-6} M^{-1}) + TBACl. Bold line; DPA G4 only. (b) Isosbestic points are observed at 365 nm (0–16 equiv of TBACl) and 371 nm (17–14 equiv of TBACl). (c) Scheme of stepwise release of $FeCl_3$. Release occurs from the periphery.

CONTROL OF ENCAPSULATION/RELEASE THROUGH FERRITIN-LIKE REDOX SWITCHING

To mimic the ferritin's function, we demonstrated the electrochemical control of the encapsulation and release of the Fe ions in the dendrimer. The reversible electrochemical reaction of $(FeCl_3)_{30}$@DPA G4 was also observed by spectroelectrochemical measurements because the time scale of the spectroelectrochemical measurement is 100 times greater than that of the CV. When Fe^{3+} was reduced to Fe^{2+} at the applied potential of –0.5 V, the absorption band around 410 nm, attributed to the complex, decreased (Fig. 8). Finally, the spectra agreed with that of the DPA G4 without Fe^{3+} ions. The resulting $FeCl_2$ is not coordinated on DPA G0 due to the weak Lewis acidity, whose association constant K is 10^8 times smaller than that of $FeCl_3$. The drastic decrease in the coordination ability results in releasing Fe^{2+} ions from the dendrimers. When the formed Fe^{3+} is applied at a potential of +0.5 V for the oxidation of Fe^{2+}, the complexation takes place. The release and encapsulation of Fe ions are reversible, which is confirmed by the same repeated spectral changes during the several redox switches. The absorption change in the release reaction obeys first-order kinetics (Fe^{2+}@imine $\rightarrow$ Fe^{2+} + imine, $k = 4.2 \times 10^{-3}$ s^{-1}, $t_{1/2} = 2.75$ min), while the complexation exhibits second-order kinetics (Fe^{3+} + imine $\rightarrow$ Fe^{3+}@imine, $k = 1.42$ s^{-1} M^{-1}, $t_{1/2} = 11.7$ min). The combination of the kinetic and the spectroscopic analyses reveals the time-controlled encapsulation and release of Fe ions in dendrimer through electrochemical switching (Fig. 9).

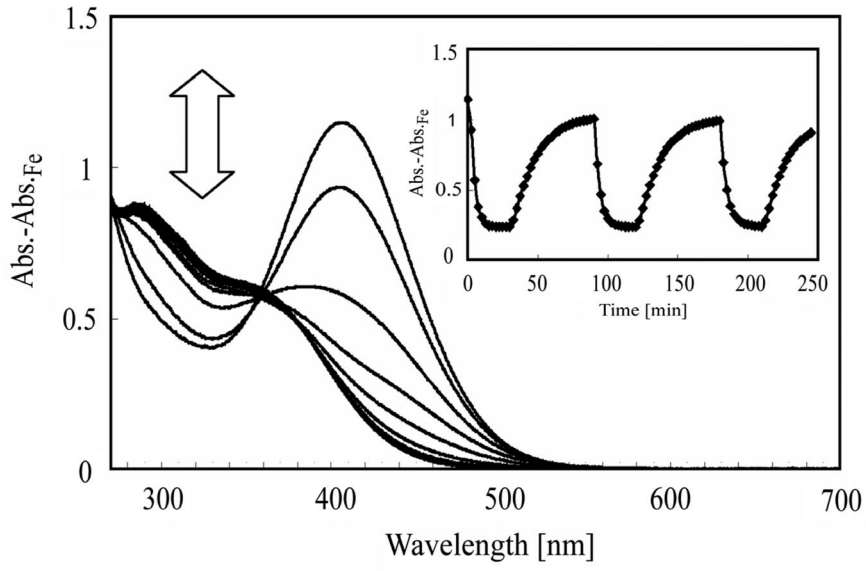

Fig. 8 Electro UV–vis spectra changes of $(FeCl_3)_{30}$@DPA G4. $FeCl_3$; 1 mM, DPA G4; 33 μM, $TBABF_4$; 0.1 M. –0.5 V ~ +0.5 V vs. Ag/Ag^+. Working; Pt wire. (Inset) Absorption changes at 410 nm. The absorption change during the release is fitted to be first-order kinetics ($k = 4.2 \times 10^{-3}$ s^{-1}, $t_{1/2} = 2.75$ min). Complexation is fitted to be second-order kinetics ($k = 1.42$ s^{-1} M^{-1}, $t_{1/2} = 11.7$ min).

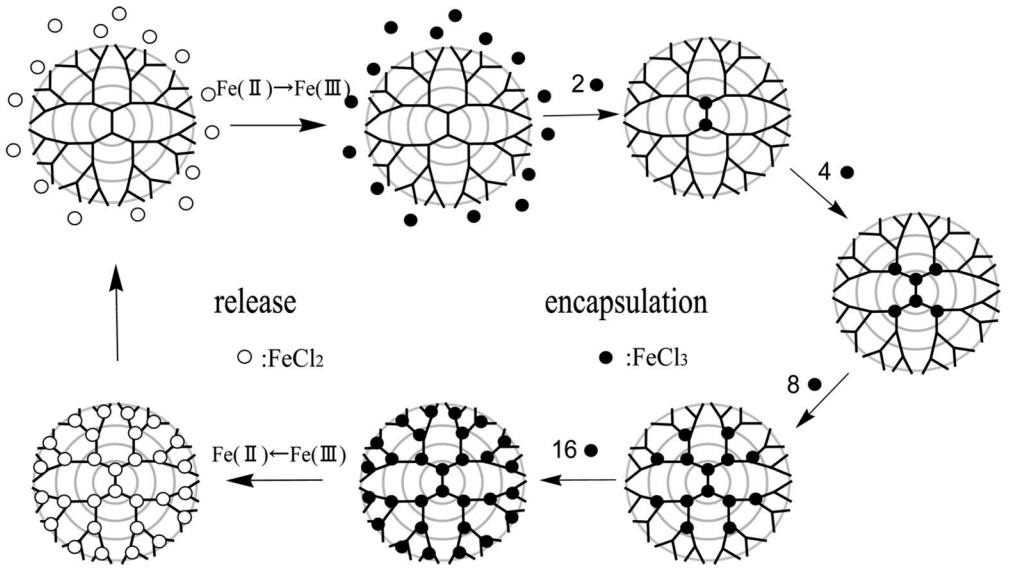

Fig. 9 Stepwise radial complexation of $FeCl_3$ and DPA G4 and Ferritin-like redox switching of Fe ion's encapsulation/release in DPA.

ASSEMBLING STRUCTURES OF THE DPA COMPLEX

A transmission electron microscopy (TEM) picture of the dendrimer complexes shows the two-dimensionally correct figure of the molecules. The ($FeCl_3$)30@DPA G4, confirmed by TEM, has a round shape with a 2.7 ± 0.35 nm diameter. Without any stain, round spots with 3.4 nm of diameter were ob-

served (Fig. 10). The dark spots are attributed to some of the Fe ions, which are similar in size to the DPA calculated by molecular modeling (2.5 × 2.9 × 2.3 nm). The existence of Fe ions was also confirmed by energy-dispersive X-ray (EDX) analysis. These results support the encapsulation of Fe ions in DPA.

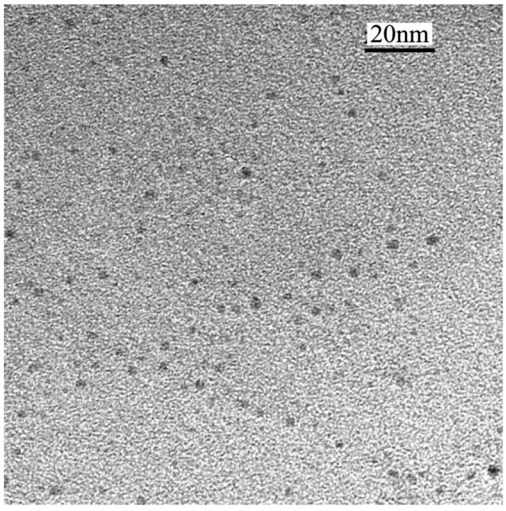

Fig. 10 TEM image of $(FeCl_3)_{30}$@DPA G4 on the grid without using any stain. Scale bar: 20 nm.

Scanning tunneling microscopy (STM) measurements demonstrated the assembling structure of Fe@DPA G4 on an osmium substrate. The $(FeCl_3)_n$@DPA G4 (n = 0, 14, 30) film was prepared by casting the $CHCl_3$ solution of the dendrimer complex on an osmium substrate. Hexagonal packing structures on the surface were observed (Fig. 11), which had repeating 3 nm DPA units in the lattice. Müllen et al. reported the assembly of dendrimers utilizing its rigid structure [20]. DPA G4 molecules also formed a packing structure because of its spherical shape and conformational rigidity [21]. The sphere-like rigid structure of the Fe@DPA complexes also results in the homogeneous film formation on an osmium plate.

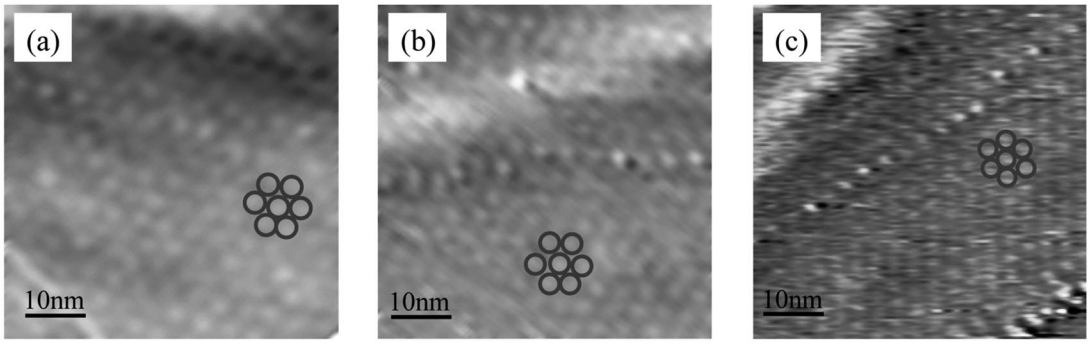

Fig. 11 STM images of $(FeCl_3)_n$@DPA G4. (a) n = 0, (b) n = 14, and (c) n = 30. Solution of $(FeCl_3)_n$@DPA G4 (5×10^{-5} M^{-1}) is cast on osmium surface (V = 950 mV, I = 50 pA).

CONCLUSION

The radial stepwise complexation with $FeCl_3$ was confirmed by UV–vis spectroscopy, electrochemistry, and mass analysis. For metal assembling, Fe^{3+} is coordinated to the imine groups from the core to the periphery and for the release, metal ions are eliminated from the periphery to the core in the DPA dendrimers. The release and encapsulation of metal ions in the dendrimer was also electrochemically demonstrated using $FeCl_3$ as a redox active metal ion. By reducing Fe^{3+} to Fe^{2+} in DPA, the Fe ions are released from DPA due to the drastic decrease in the Lewis acidity. This system acts as a mimic function of the Fe storage protein ferritin and an advanced drug delivery system. The rigid and sphere-like structures were confirmed, which result in multilayers with a hexagonal packing. Only solvent casting of the Fe@DPA solution provides a well-ordered homogeneous film substrate, which can be used to easily fabricate devices.

REFERENCES

1. D. A. Tomalia, H. Baker, J. Dewald, H. Hall, G. Kallos, S. Martin, J. Roeck, J. Ryder, P. Smith. *Polym. J.* **17**, 117 (1985).
2. G. R. Newkome, Z. Q. Yao, G. R. Baker, V. K. Gupta. *J. Org. Chem.* **50**, 2003 (1985).
3. S. M. Grayson, J. M. J. Fréchet. *Chem. Rev.* **101**, 3819 (2001).
4. A. W. Bosman, H. M. Janssen, E. W. Meijer. *Chem. Rev.* **99**, 1665 (1999).
5. F. Vögtle, S. Gestermann, R. Hesse, H. Schwierz, B. Windisch. *Prog. Polym. Sci.* **25**, 987 (2000).
6. R. M. Crooks, M. Zhao, L. Sun, V. Chechik, L. K. Yeung. *Acc. Chem. Res.* **34**, 181 (2001).
7. J. W. Knapen, A. W. van der Made, J. C. de Wilde, P. W. N. M. van Leeuwen, P. Wijkens, D. M. Grove, G. van Koten. *Nature* **372**, 659 (1994).
8. M. T. Morgan, M. A. Carnahan, C. E. Immoos, A. A. Ribeiro, S. Finkelstein, S. J. Lee, M. W. Grinstaff. *J. Am. Chem. Soc.* **125**, 15485 (2003).
9. A. V. Ambade, E. N. Savariar, S. Thayumanavan. *Mol. Pharm*. **2**, 264 (2005).
10. W. Kaim, B. Schwederski. *Bioinorganic Chemistry: Inorganic Elements in the Chemistry of Life: An Introduction and Guide*, John Wiley, Chichester (1994).
11. M. A. Zapien, M. A. Johnson. *J. Electroanal. Chem.* **494**, 114 (2000).
12. M. S. Rao, I. S. Dubenko, S. Roy, N. Ali, B. C. Dave. *J. Am. Chem. Soc.* **123**, 1511 (2001).
13. Z. D. Hill, P. MacCarthy. *J. Chem. Educ*. **63**, 162 (1986).
14. K. Yamamoto, M. Higuchi, S. Shiki, M. Tsuruta, H. Chiba. *Nature* **415**, 509 (2002).
15. K. Takanashi, H. Chiba, M. Higuchi, K. Yamamoto. *Org. Lett.* **6**, 1709 (2004).
16. R. Nakajima, M. Tsuruta, M. Higuchi, K. Yamamoto. *J. Am. Chem. Soc.* **126**, 1630 (2004).
17. M. Rudolph, D. P. Reddy, S. W. Felberg. *Anal. Chem.* **66**, 589A (1994).
18. A. J. Bard, L. R. Faulkner. *Electrochemical Methods: Fundamentals and Applications*, John Wiley, Chichester (2000).
19. T. L. Chasse, R. Sachdeva, Q. Li, Z. Li, R. J. Petrie, C. B. Gorman. *J. Am. Chem. Soc.* **125**, 8250 (2003).
20. C. G. Clark Jr., R. J. Wenzel, E. V. Andreitchenko, W. Steffen, R. Zenobi, K. Müllen. *J. Am. Chem. Soc.* **129**, 3292 (2007).
21. M. Higuchi, M. Tsuruta, H. Chiba, S. Shiki, K. Yamamoto. *J. Am. Chem. Soc.* **125**, 9988 (2003).